Multi-Objective Design
of a Biodegradable Coronary Artery Stent

Neil W. Bressloff

Abstract Ever since the mid 1980s when the first-in-man coronary stent procedure was conducted, commercially available coronary stents have evolved from the original stainless steel Palmaz-Schatz style of design to a range of highly flexible, slick structures capable of providing arterial support with very thin struts. The availability of modern alloys such as platinum-chromium has facilitated the evolution to thin strutted, highly flexible devices. However, an important juncture has been reached wherein the combination of thin struts and low numbers of stent links/bridges has introduced a new challenge associated with loss of longitudinal strength. Interestingly, this has coincided with an increasing focus on the use of biodegradable materials (e.g., polymers or magnesium). So, whilst polymer scaffolds currently require relatively thick struts, it might be anticipated that efforts will be made to develop stronger polymers also leading to thinner struts, but with the awareness of the pitfalls associated with emphasis on particular measures of performance (objectives) at the expense of others. In parallel with the evolution of coronary stents, computational methods (and hardware) have developed to a point whereby optimization and simulation tools can now be used to systematically design devices in a realistic time-scale. This chapter demonstrates how these tools can be harnessed to guide the multi-objective design process, with the ultimate aim that superior prototypes, particularly those that are biodegradable, can be designed and refined computationally.

N. W. Bressloff (✉)
Institute for Life Sciences, University of Southampton,
Highfield, Southampton SO17 1BJ, UK
e-mail: nwb@soton.ac.uk

1 Introduction

Now that metallic stents are approaching a mature stage of evolution and advances in the development of biodegradable scaffolds are supporting the realization of a fourth revolution in interventional cardiology [1], it is timely to consider what lessons have been learnt from the design of permanent metallic devices, and how best practice might be applied to the development of a growing number of polymeric scaffolds, in particular.

Interventional cardiology was first revolutionized in the 1970s when Andreas Gruntzig and colleagues performed the first human coronary balloon angioplasty in 1977. The second revolution occurred in the mid 1980s with the introduction of bare metal stents; even though the Palmaz-Schatz stent was not approved by the Food and Drug Administration (FDA) in the United States until 1994. Nearly a decade later, FDA approval was granted for Johnson & Johnson's Cypher drug eluting stent (DES), signifying a key milestone in the third revolution in interventional cardiology. DESs represent the current state of the art and a useful review of DESs is available in [2]. Whilst most widely available stents are deployed using balloon inflation [3], there is also a range of self-expanding devices which also emerged in the 1990s [4]. Three of the most popular DESs are listed in Table 1 along with the *Cypher* platform and Abbott Vascular's second generation bioresorbable vascular scaffold, *BVS-B*. The *BVS-B* device is one of the major forerunners in the fourth revolution which started in the early to mid-1990s with tests of non-biodegradable and degradable polymers in porcine animal models [5, 6] and with the first-in-man procedure of the fully biodegradable Igaki-Tamai coronary stent in 1998. Early results were presented by Tamai, Igaki and others in 2000 [7].

Some key questions are inevitably posed when considering the evolution of stent design and the implications for fully biodegradable devices. For example: (i) is there sufficient justification for stents that perform the necessary function and then disappear (within approximately 2 years)?; and (ii) will it be possible to develop strong enough polymeric stents, capable of treating the wide range of challenging disease states routinely encountered in the cath-lab? With respect to the first question, there is an increasing body of evidence to support the positive claims of Serruys [1] and others [8], including the long-term evidence (based on a follow-up study lasting more than 10 years) of the first-in-man Igaki-Tamai stents for safe and effective treatment using bioresorbable scaffolds [9], and the recent identification of late positive remodeling and late lumen gain [10], and the implications for the recovery of normal vasomotion. Indeed, there are a number of compelling reasons for favoring the biodegradable scaffold concept over that of the metallic cage.

Despite these encouraging findings, the second question above brings a major issue into focus concerning the material properties of currently available polymers and the geometric constraints associated with them. Whilst platinum-chromium has an elastic modulus, $K = 203$ GPa, the value reported for the polymer used in

Table 1 Comparison of stent platforms

Platform	Company	Material	Elastic modulus (GPa)	Strut thickness (μm)
BVS-B	Abbott Vascular	PLLA	3.3	150
Cypher	Johnson & Johnson	316L SS	193	140
Element	Boston Scientific	PtCr	203	81
Endeavor	Medtronic	CoCr	210–243	90
Xience	Abbott Vascular	CoCr	210–243	81

PLLA poly-l-lactic acid. *SS* stainless steel, *PtCr* platinum-chromium alloy, *CoCr* cobalt-chromium alloy

the Abbott Vascular *BVS-B* device is $K = 3.3$ GPa. 316 L stainless steel has $K = 193$ GPa.

Due to the low stiffness of polymers, all currently known scaffolds have significantly thicker struts than modern metallic stents; for example, the *BVS-B* scaffold has a strut thickness, $t = 150$ μm (0.150 mm) and, in trials, is being restricted to relatively straightforward, non-calcified *de novo* lesions [11]. From the thicknesses listed in Table 1, it is clear that significant research is necessary to bridge the gap between polymeric and metallic materials. For reference, the original Igaki-Tamai stent had a thickness of 170 μm.

However, a further question comes to mind at this point: how will long term performance compare between devices made from the different materials, bearing in mind that the merits of biodegradable scaffolds may more than compensate the geometric disadvantages (e.g. thicker and wider struts) necessitated by inferior material properties? Additionally, the trend towards thinner, narrower struts has recently led to a new problem of stent distortion [12, 13], a phenomenon highlighting the need to carefully consider multiple measures of performance. In this case, the drive towards thinner struts and greater flexibility has dominated all other considerations and has resulted in devices with compromised longitudinal strength. Indeed, the recognition that stent design involves a number of potentially conflicting performance metrics (or objectives) is allied in this chapter to the tools (computational and experimental) that are available to both simulate device performance and to steer the design process itself.

Section 2 focuses on the evolution in design of metallic stents, primarily with respect to geometry. In Sect. 3, currently known biodegradable scaffolds are described and mainly geometric comparisons are made in terms of key defining features. Design methodologies are considered in Sect. 4, including how they might be best exploited in the development of polymeric devices.

2 Evolution in Design

When considering the evolution of coronary stent design, it is immediately apparent that two key geometric differences have emerged relative to the Palmaz-Schatz device: (i) open cells and (ii) thinner struts. The original Palmaz-Schatz
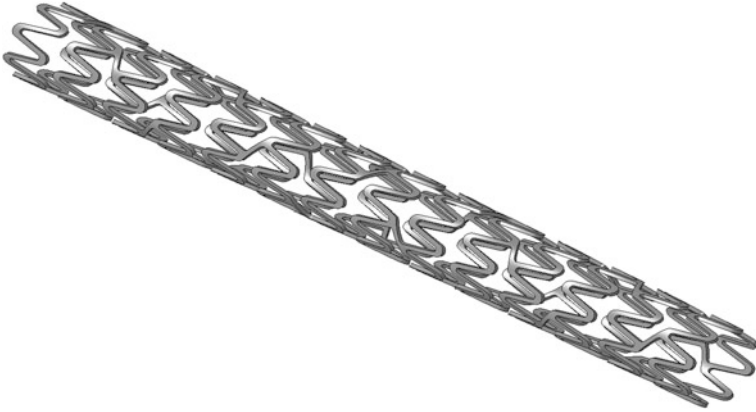
Fig. 1 CAD model of the Boston Scientific *Element* platform

stent had a thick strut, closed cell configuration. Over the years, it has been established that thinner struts reduce the likelihood of in-stent restenosis [14] and greater flexibility and conformability are achievable with open cell designs [15]. Reduced strut dimensions have been made possible by the introduction of modern alloys (including platinum-chromium, cobalt–nickel and cobalt-chromium) [1] allied to advances in manufacturing processes.

Just before the introduction of drug eluting stents, Stoeckel et al. conveniently categorized and differentiated the large number (approximately 100) of stents "being marketed or in evaluation worldwide" [16]. Stoeckel et al. suggested that the stent market would double from $3 billion "with the advent of drug eluting stents" [16]. At approximately the same time, a wide range of stents were appraised in [17]. Although there are still multiple variants of stent design, all probably motivated by intellectual property and commercial considerations, there has been significant convergence in design features towards open cell configurations, comprising rings and links/bridges/connectors (see Figs. 1, 2 in [13]) all cut by laser from thin metallic tubes and deployed by balloon inflation on a catheter. Fig. 1 shows a representative model, constructed in the Rhino Computer Aided Design (CAD) package (Robert McNeel & Associates), of the Boston Scientific *Element* platform. This represents one of the simplest manifestations (in terms of geometry) of the ring-link topology, with just two inclined bridges joining adjacent rings.

Two notable exceptions to this classification should be mentioned here: (i) Medtronic's *Integrity* platform since it is manufactured from a continuous wire and not cut from a tube, and (ii) the group of self-expanding, Nitinol stents including the STENTYS product [18]. Nonetheless, variation in design primarily exists in the relative positions of the peaks in adjacent rings and in the shape and alignment of the links between adjacent rings. Significant non-geometric differences include the platform material and the drug constituents in DESs.

So, even though it is not surprising that many different products are available in a competitive market, it is encouraging to observe, especially from the patient's
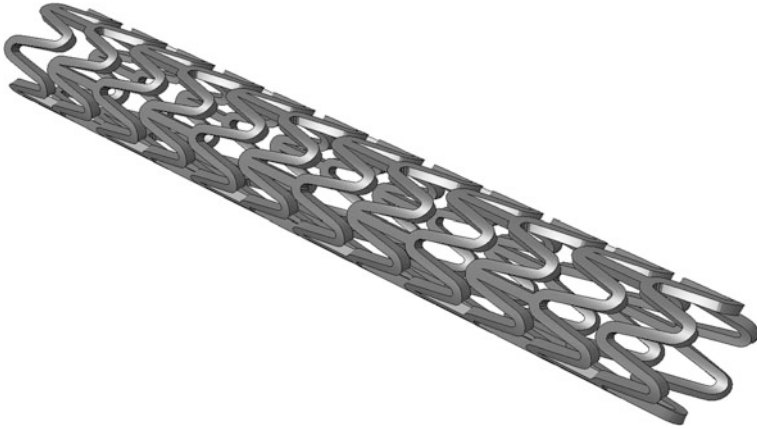
Fig. 2 Generic polymer scaffold with in-phase rings joined by straight bridges (based on the *BVS-B* platform)

perspective, that convergence in (geometric) design has taken place. Divergence (mutation) in design is also to be expected, and so niches in the market exist for self-expanding devices, for example, and other "mutations". Continuing the evolutionary analogy, it might be expected that new "species" could emerge and evolve to become market leaders. Indeed, the fourth revolution in interventional cardiology could result in bioresorbable scaffolds dominating the market. Conveniently, this family of devices is at a relatively early stage of development and so it is instructive to consider their geometric features, in particular, and to explore how design techniques can be exploited to steer their evolution. Since there are only a modest number of devices that have been publicized and shown to have reached a reasonable level of development, and even fewer that have entered clinical trials [19], a survey equivalent to the one by Stoeckel et al. may be a little premature. Nonetheless, inspired by the "stent design pyramid" in [16], the next section focuses on the geometry slice adjacent to the base of the pyramid.

3 A Survey of Bioresorbable Scaffold Geometry

Bourantas et al. [19] have presented a recent survey of bioresorbable scaffolds, principally focusing on ongoing clinical trials. Sufficient information is known concerning 10 scaffolds, each being developed by separate companies, and there are at least another five companies that are involved in the development of biodegradable scaffolds. These are Arterius Ltd (UK), Meril Life Sciences (India), Sahajanand Medical Technologies Pvt Ltd (India), S3 V Vascular Technologies Pvt Ltd (India) and Zorion Medical (US).

Table 2 Geometry configurations of known bioresorbable scaffolds

Scaffold name	Company	Cells	Rings	Links
ABSORB BVS-B	Abbott Vascular	Open	In-phase	Straight bridge
Acute	Orbus-Neich	Hybrid	–	Inclined bridge
ART18AZ	Arterial Remodelling Tech.	Hybrid	Out-of-phase	Straight bridge
Amaranth PLLA	Amaranth	Open	In-phase	Straight bridge
DESolve BCS	Elixir Medical Corp.	Open	In-phase	Straight bridge
DREAMS2	Biotronik	Open	In-phase	Wavy mid-strut
Ideal BioStent	Xenogenics	Open	In-phase	Straight bridge
Igaki-Tamai	Kyoto Medical Planning Co.	Open	Out-of-phase	Inclined bridge
ReZolve2	Reva	Slide & lock	–	–
Xinsorb	Huaan Biotech.	Open	Out-of-phase	Straight bridge

Due to the very different material properties of the polymers and metal alloys used to manufacture stents, it is important to consider whether the respective devices should be designed in the same way. However, much has been learnt over the last 20 years concerning stent geometry, and it is not by chance that many state-of-the-art devices have now converged to similar recognizable configurations; i.e., adjacent circumferential wavy rings joined by an arrangement of links/ bridges/connectors. With the appropriate wave amplitude (i.e. longitudinal wave height) and wavelength (i.e. controlled by the number of circumferential peaks/ crowns), plastic deformation occurs in the peaks during expansion from diameters of approximately 1 mm to a few mm, such that the device can withhold its expanded shape even when exposed to the elastic loading of a host vessel. So, whilst it might be argued that polymeric stents should *not* be designed in the same way as the well-established metallic counterparts, this is not largely apparent in practice. The understanding and proven performance of ring and link configurations is now being exploited in the designs of the majority of polymeric scaffolds and at least seven of them can be identified in this way (also see Table 2):

ABSORB BVS-B: in-phase rings joined by three longitudinally in-line, straight bridges. Fig. 2 depicts a model (constructed in the Rhino CAD package) of a generic platform with in-phase rings joined by three straight bridges.
ART18AZ: out-of-phase rings. Alternating pairs of rings are joined at all peaks by a very short bridge or at only two peaks which are positioned in a longitudinal spiral arrangement. Fig. 3 shows a CAD model based on the *ART18AZ platform.*
Amaranth PLLA: in-phase rings joined by three longitudinally in-line, straight bridges.
DESolve BCS: in-phase rings joined by three longitudinally in-line, straight bridges.
Ideal BioStent: in phase rings joined by three longitudinally in-line, straight bridges.
Igaki-Tamai: out-of-phase rings joined by three helically arranged short bridges.
Xinsorb: out-of-phase rings, each pair joined by three short straight bridges, longitudinally in-line.
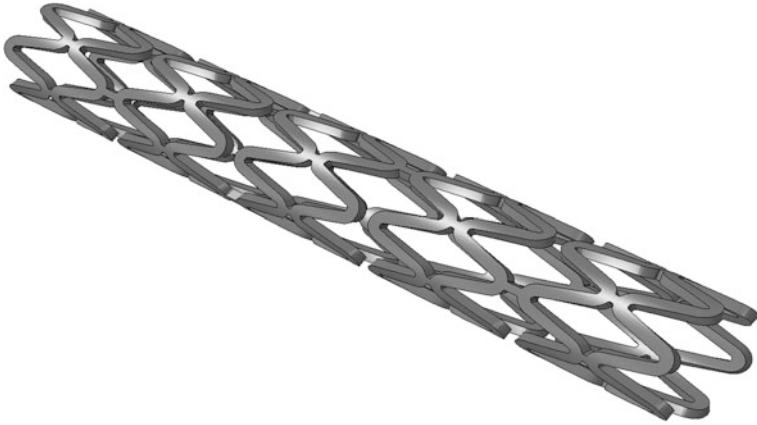
Fig. 3 Generic polymer scaffold with out-of-phase rings (based on the *ART18AZ* platform)

Thus, there are four polymeric devices with in-phase rings and three with out-of-phase rings. The four in-phase devices are topologically very similar, although the *Ideal BioStent* differs due to having very wide struts.

The three out-of-phase devices have more significant differences with respect to the arrangements of bridges between adjacent rings. In particular, the *ART18AZ* design has alternating pairs of rings that form arrays of closed and open cells (c.f. Fig. 3).

The *Acute* device (Orbus-Neich) is less obviously defined in the same way as the seven above. However, in its expanded shape, it can be described as comprising arrays of closed cells (formed by pairs of adjacent rings) with each array joined by three inclined, longitudinal bridges. Since the lengths of the bridges are comparable to the longitudinal length of each closed cell array, it can be classified as a hybrid device.

The two remaining well known biodegradable scaffolds have significant characteristics that distinguish them from the other eight. The *ReZolve2* device (Reva Medical) is polymer based and balloon expandable, but it has a unique slide and lock mechanism. The *DREAMS2* device (Biotronik) is the only non-polymeric bioresorbable scaffold; made from magnesium alloy, it looks like a conventional metallic stent. Geometrically, it can be classified as an open cell device with wavy, in-phase rings joined by wavy mid-strut links.

Most of the information described above has been obtained directly from company internet pages and complemented by images and details in the literature [13, 19]. Accurate dimensions have not been obtained for all platforms and, in general, only strut thicknesses are publicly available. Based on the available data, all known thicknesses range between 150 and 200 μm for polymeric devices, but the magnesium alloy *DREAMS* device is 125 μm thick. As discussed above, these thicknesses are significantly larger than those for state-of-the-art permanent metallic stents. This suggests that current and future research is likely to focus on reducing the thickness (and the width) of bioresorbable scaffolds. Essentially,

material strength needs to be increased through tube/material treatment, additives and/or other methods. Durand et al. have recently demonstrated the effect of co-polymer composition on radial strength and biocompatibility, albeit still at relatively low levels of material stiffness [20]. As advances are made, opportunities will emerge to further enhance the geometries of the underlying platforms, and therein lays the possibility to efficiently develop optimal designs using design optimization tools and high performance computing [21].

4 The Design Process

When undertaking a design study (experimental and/or computational) it is likely that a finite number of different designs can be assessed and compared in the search for an optimal design. This is particularly the case in industry where commercial demands normally restrict the time available to develop a product. Often, satisfactory design improvement is accepted whilst recognizing that too much time would be needed to find the best of all designs. Hence, the designer has to formulate how many different design realizations can be tested in the available time and this depends on

(i) the design methodology (and problem fidelity);
(ii) parameterization (the inputs); and
(iii) measures of performance (the outputs).

Since the focus here is on the computational design of coronary artery stents, these dependences are now considered in this respect, thus introducing a further, specific (modeling) dependency: the availability and power of computers and software. In contrast, a laboratory experimental approach is dependent on the effectiveness of available testing equipment.

4.1 Design Methodology (and Problem Fidelity)

Most coronary stents are supplied pre-crimped on a catheter, so the deployment of balloon inflated coronary stents involves positioning with the aid of angiography, followed by expansion through high pressure filling and inflation of the balloon using a contrast agent. It is possible to simulate the complete interventional procedure using finite element analysis (FEA), although the positioning step is only occasionally included [22], balloons are sometimes replaced by a displacement boundary condition [23] and balloon inflation is controlled by surface pressure applied to the inner surface of the balloon. Although real devices are pre-crimped before delivery to the cath-lab, the crimping procedure can also be simulated in order to capture the pre-strain it generates [24, 25]. At the very least, the structural deformation of the stent is simulated. However, simulations of free expansion ignore
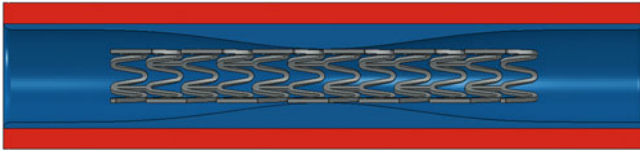
Fig. 4 Representative diseased artery segment before stent deployment

the important interaction that occurs in contact with a diseased host vessel. Relative to this low level of fidelity, high fidelity simulations include crimping, positioning and balloon expansion (see Figs. 5, 6, 7, 8 below) inside a vessel comprising plaque and the artery wall, both modeled by appropriate constitutive formulations [26]. The vessel may be representative [21] or based on a real patient [27].

Figure 4 depicts a representative diseased segment. Such models are relatively simple and fast to setup and manipulate, all within CAD software. Here, the constriction shape is based on a Hicks-Henne definition [28].

In contrast, Fig. 5 shows a reconstructed, patient specific right coronary artery segment. Using a time consuming manual process, a set of intravascular ultrasound (IVUS) slices have been combined with two approximately orthogonal angiogram projections, all obtained in Southampton General Hospital cath-lab. This model has been setup in preparation for ongoing patient specific design studies at the University of Southampton, UK.

Also shown in Fig. 5 are models of the Boston Scientific *Element* stent platform, catheter and guide wire. As mentioned above, a high fidelity simulation involves crimping, positioning and expansion. For this model, preliminary tests have been successfully completed for these steps in Abaqus Explicit 6.11.1. Figures 6, 7, 8 show snap-shots in the three steps.

First, the stent is crimped onto a catheter (c.f. Fig. 6) using an external surface (not shown) with an applied displacement boundary condition on its outer surface. The stent is assumed to be made from the platinum-chromium alloy with an elastic modules of 203 GPa, Poisson ratio of 0.35 and yield stress of 455 MPa.

Once crimped, the stent is moved into position (c.f. Fig. 7) by applying a displacement boundary condition on the proximal end of the catheter. A contact definition between the catheter and the guide-wire forces the catheter to follow the line of the guide-wire, fixed according to the position extracted from the original IVUS images.

Figure 8 depicts the final deployed position of the stent following expansion using a surface, again controlled by a displacement boundary condition. This surface approach offers a faster simulation alternative to modeling the inflation of a balloon [24]. The tissue is modeled as a hyperelastic material using the Holzapfel strain energy potential constitutive model in Abaqus 6.11.1.

In addition to the simulations described above, it may also be necessary to perform other simulations for flow disturbance (using computational fluid dynamics (CFD)) [29] and other structural considerations (e.g. flexibility, fatigue, longitudinal strength) [11].

Fig. 5 Patient specific right coronary artery segment. A Boston Scientific *Element* stent model is also shown before crimping on a catheter, guide-wire system

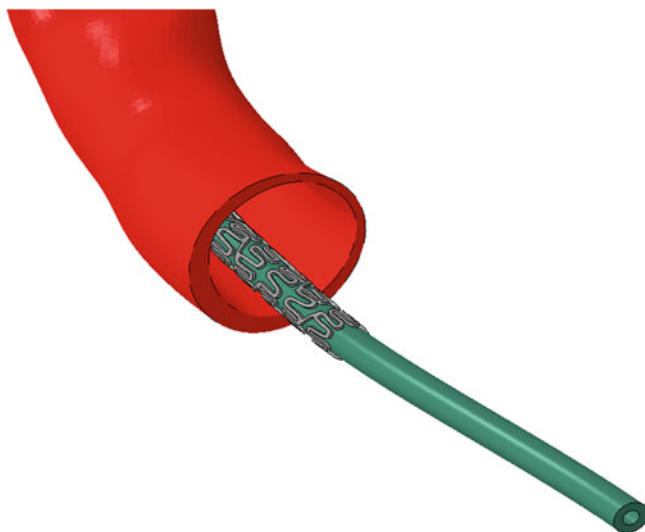**Fig. 6** Crimping of the Boston Scientific *Element* stent model

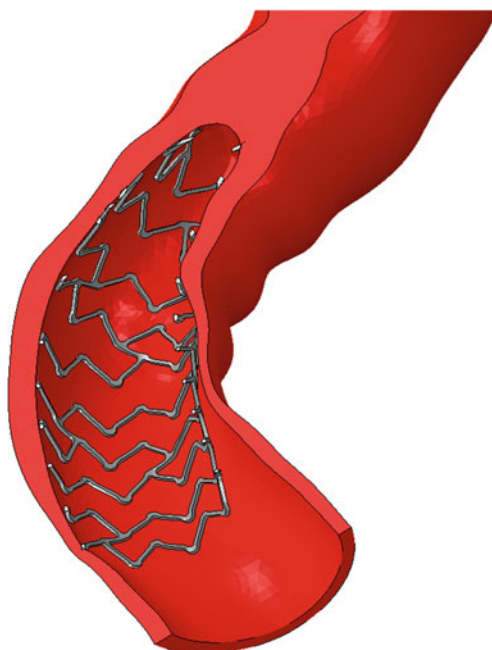**Fig. 7** Positioning of the Boston Scientific *Element* stent model

Fig. 8 Expansion of the Boston Scientific *Element* stent model

The time to run simulations of a single design can differ by two orders of magnitude or more. Thus, depending on the amount of time available, a decision has to be made concerning the level of fidelity to use. If a relatively high level of fidelity is required, a number of days are likely to be needed to simulate a single design realization [21] (even when using parallel computing on high performance computers). In contrast, sixty single ring configurations were simulated overnight using low fidelity simulations in [30]. Software licensing may also constrain the speed of computation by restricting the number of parallel licenses that can be used.

4.1.1 Surrogate Modeling

When individual simulations are expensive, the most appropriate way to perform design search and optimization (DSO) involves the response surface methodology wherein a surrogate model (or response surface) is constructed to represent the relationship between design outputs (measures of performance) and design inputs (parameters, often geometry based). Fig. 9 depicts the key steps in response surface modeling. These are shown on the left hand side of the chart (numbered 1–7), whereas the box on the right hand side describes the process of modeling individual designs.

(1) Starting from a new concept, it is necessary to construct a CAD model of the baseline stent. Typically, this is likely to involve hands-on manipulation of shapes using a graphical user interface (GUI), combined with the development of a computer script (or code). Ideally, the script can completely construct the model as a batch process without opening the GUI. This automated approach is favored since significant time can be saved by not having to manually craft individual designs.

(2) During model construction, a number of variables are likely to be setup, but only a relatively small number of them are defined as input parameters (c.f. Sect. 4.2). For each parameter, an appropriate range of acceptable values has to be defined by upper and lower bounds. Similarly, decisions are made at this stage for the measures of performance (or outputs) to be used (c.f. Sect. 4.3) and whether any constraints are to be defined. Also, problem definition and setup requires the appropriate simulation approaches to be setup, tested, verified and validated if possible.

(3) Having constructed a baseline configuration and defined the parameterization, it is now necessary to identify a family of designs (based on the baseline) that is to be analyzed. This initial sample needs to be appropriately distributed throughout the design space and a number of space-filling algorithms (or design of experiments) are available to do this. Decisions concerning the selection of a particular design of experiment and the size of the sample are discussed in [31].

(4) Analysis of each design involves three key stages: (a) model construction including setup of the mesh, boundary conditions and initial conditions;
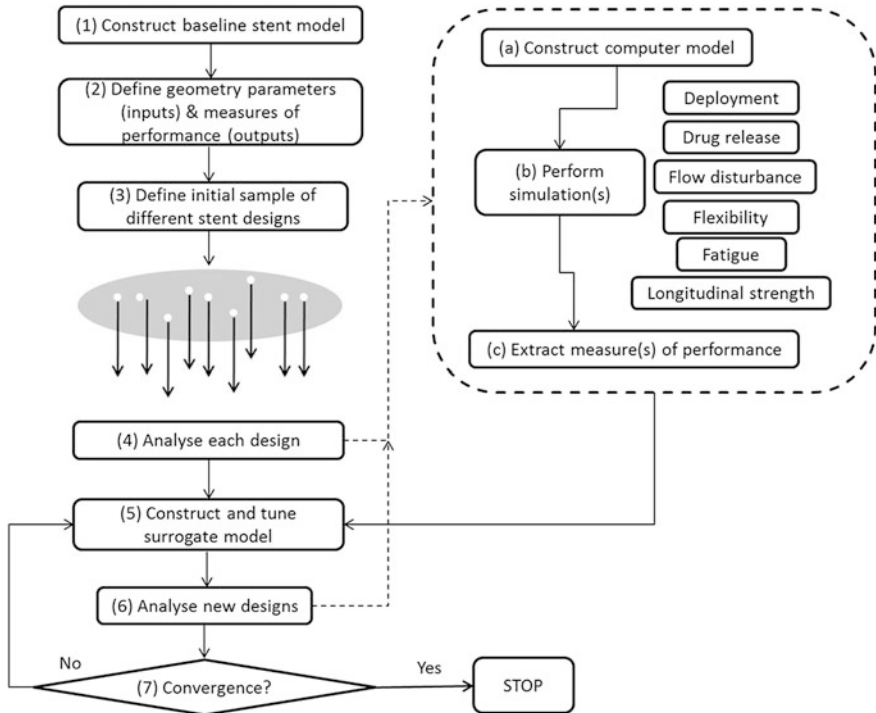
Fig. 9 Flow chart showing the process of surrogate modelling

(b) simulation(s) and (c) post-processing of the simulation(s) to extract appropriate measure(s) of performance. In most cases, some form of deployment simulation is included and then one or more of the other simulations (e.g. CFD, flexibility) are conducted, dependent on the measure of performance needed.

(5) Construction (and tuning) of the surrogate model involves the evaluation of hyper-parameters used in the mathematical formulation of the surrogate model, by substituting the inputs and associated outputs into this formulation. In other words, the surrogate model is a generic mathematical function with unknown terms (or hyper-parameters) that have to be evaluated for the known inputs and outputs, respectively defined and obtained, for the family of designs simulated in step (4). Tuning of the surrogate model is normally required so as to improve its accuracy. Based on the inputs and outputs, tuning maximizes the likelihood that the model reproduces the known outputs for the given inputs. The preferred choice of surrogate model, and the one used to generate the response surfaces shown in this chapter, is Kriging [32, 33], popularized in [34].

(6) Once the model has been constructed it can be searched and tests performed to identify where new designs should be analyzed. So-called update points are then added to the family of designs used to construct the original model.

Normally, the same simulations as were used for the initial sample are performed for each new analysis.

(7) Termination of the process occurs when a suitable level of convergence is reached in the surrogate model and/or the available time for the design process is exhausted. If additional designs need to be analyzed, and time is available, further simulations are performed and the surrogate model is re-constructed. This loop is repeated until convergence. In Sect. 5, a time-limited design study is described for one of the new generation of biodegradable devices.

4.2 Parameterization

Parameterization often involves geometry variables appropriately setup so that a family of different designs can be generated and compared. For a given coronary stent design concept, these variables are likely to define the shapes of the crowns, links and strut cross-section. In [30], five shape parameters were varied: strut width, strut thickness, crown radius, strut length and weld radius. Pant et al. kept strut thickness constant in their study of a generic closed ring metallic stent and assessed the effect of strut width, ring length (equivalent to strut length) and two parameters that define the wavy links [25]. Experience in this work led to a three parameter assessment of the *Cypher* platform in which the wavy links were controlled by a single parameter [21].

In contrast to the direct manipulation of geometry parameters, Wu et al. controlled the shape of a single stent ring unit by moving mesh nodes in a pre-meshed baseline model and used a mesh morphing procedure to maintain a good quality mesh in the morphed shapes [35]. There are also a number of other shape control methods that can be used including free form deformation and spline and surface control point manipulation. Further consideration of optimisation studies is included in [21].

4.3 Measures of Performance

Radial strength often represents the key design objective since, unless a device can resist the elastic recoil of the vessel it is meant to support, other measures of performance are not worth consideration. Fig. 10 shows three stages in the simulation of expansion of the model of the *BVS-B* platform originally shown in Fig. 2. An elastic membrane (representative of a semi non-compliant balloon) is inflated into contact with the inner surface of the stent as shown in Fig. 10a. Note the dog-boning effect at the end of the stents. In Figs. 10b, c, respectively, the stent is shown in its fully expanded and final (post recoil) states. The balloon material has been removed from these views so that the expanded stent can be clearly seen.
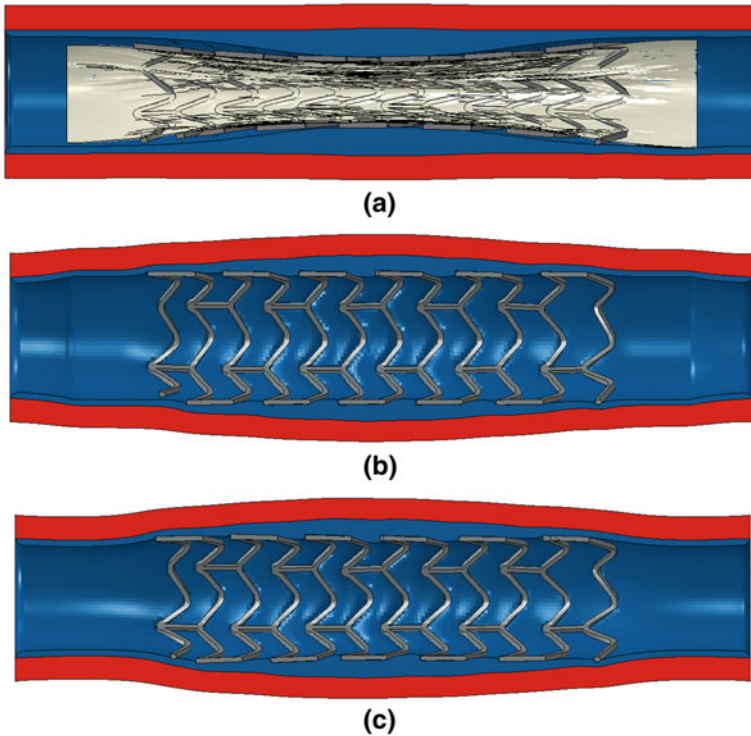
Fig. 10 Expansion and recoil of the *BVS-B* model: **a** balloon inflation; **b** fully expanded; **c** recoil

In this simulation, the polymeric stent had an elastic modulus of 3.363 GPa, a Poisson ratio of 0.45 and a yield stress of 40 MPa. A Neo-Hookean hyperelastic model was assumed for the plaque with shear modulus 0.12 MPa and bulk modulus 1.7 MPa, whilst the single layer artery was assumed to be a hyperelastic material with a six order reduced polynomial strain energy density function. The stent, plaque and artery all had 8-noded linear hex elements. Finally, the balloon was modelled as an elastic membrane with an elastic modulus of 1400 MPa, a Poisson's ratio of 0.3, a thickness of 0.05 mm and was meshed with 4-noded membrane elements. Further details and justification for these models is available in [25].

Figure 11 shows maximum expansion and final recoiled deformation of the *ART18AZ* model, using the same settings as for the *BVS-B* model. The deformations of the *ART18AZ* device appear to be less satisfactory than those of the *BVS-B* device with inferior scaffolding, noticeable prolapse and approximately double the amount of recoil (relative to the respective fully expanded shapes).

Although the *BVS-B* model appears to out-perform the *ART18AZ* model with respect to recoil, this may be due to inaccuracies of the underlying CAD models. For example, there is noticeable distortion in the cells of the *ART18AZ* model which could be the result of poor geometry representation (recall that these models were constructed just using inspection of publically available images). However,
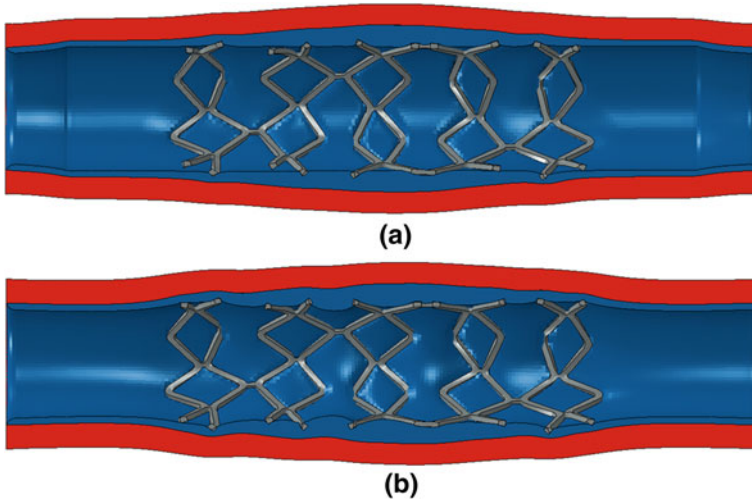
Fig. 11 Expansion and recoil of the *ART18AZ* model: **a** fully expanded; **b** recoil

there is potential concern with respect to having only two bridges joining adjacent rings, in light of the known longitudinal compression problems particularly associated with the Boston Scientific *Element* platform.

In addition to radial strength, devices need to be as flexible as possible for deliverability and conformability. For drug eluting stents, it is favourable to optimize the drug distribution within arterial tissue. Indeed, the clinical control of inflammation and smooth muscle cell proliferation demand consideration of (i) the potential injury to the arterial tissue resulting from the stresses imposed by stent struts embedded into the vessel wall and (ii) the disturbance to the flow and the associated wall shear stress to which the endothelium is exposed. So, metrics are needed for the stresses within the tissue and the (shear) stresses on the surface of the vessel.

In [25], four measures of performance were considered in the DSO of a generic closed cell stainless steel stent: (i) recoil; (ii) tissue stress; (iii) drug distribution and (iv) flexibility. A further two objectives were included in an optimization analysis of the *Cypher* platform [21] to represent flow disturbance and the uniformity in drug distribution. Thus, relative to the study in [25] the additional objectives required a CFD simulation and further post-processing for the variance in drug concentration.

For the study of biodegradable magnesium alloy stents, Wu et al. adopted a twin objective approach (side-stepping the multi-objective problem) whereby the effects of maximum principal strain and mass on biodegradability were recognized. The maximum principal strain was minimized first and then mass (strut width) was maximized by selecting the design with highest mass from all the designs for which the maximum principal strain was less than a prescribed limit [35].

4.4 Multi-Objective Design

If more than one measure of performance is used, the multi-objective design problem often requires trade-off considerations to be made; typically, an improvement in one objective correlates with a deterioration in another. With more than two objectives, both positive and negative correlations can exist simultaneously between different pairs of objectives.

As described above, the multi-objective problem can be avoided when, for example, it is possible to rank objectives a priori [35]. Alternatively, the optimization can be recast as a constrained problem, wherein design improvement is sought in one objective whilst ensuring that other objectives don't deteriorate [25]. Although Pant et al. did not present response surfaces in [25], it is useful to present and discuss them here. The stent parameterisation and the full set of results are available in [25]. The intention here is to demonstrate the way that multi-dimensional design spaces can be presented and interpreted.

So, Fig. 12 depicts the variation in non-dimensional stent recoil against non-dimensional strut width (plotted on the abscissa of each inner tile), non-dimensional strut length (inner tile ordinates), non-dimensional link amplitude (outer abscissa) and non-dimensional link wavelength (outer ordinate). This plot has been created using the Kriging response surface formulation. Since there is only a very slight variation between each tile, this shows that the link parameters have little effect on recoil. The strongest effect is produced by the strut width, whereby wider struts provide greater vessel support.

In contrast to recoil, tissue stress is minimized by narrow struts as shown in Fig. 13. Again, the link parameters have little effect, but strut length has a noticeable impact at large values of strut width, i.e. tissue stress is maximized when both width and length are high. This is to be expected since tissue stress is based on a volume averaged integral which increases with the higher radial force associated with lower recoil.

Since the delivery of drug depends on surface contact, it is to be expected that drug concentration in the tissue is positively correlated with tissue stress. Cast as a minimization problem, the variation in the inverse of drug concentration is depicted in Fig. 14. In general, wider struts predict better drug delivery, but strut length has an unexpected impact. At low values of strut width, it is clear that increasing strut length leads to higher concentrations of drug. However, at high values of strut width, variation in strut length has a negligible effect. This is due to the dependence of the total contact area (including the contribution from the links) on strut length. Since the overall length of the stent is constant, variation in strut length leads to variation in the total arc length of the links and, hence, the contact area.

The fourth objective is flexibility and its non-dimensional variation is shown in Fig. 15. This is an apparently confusing response, largely resulting from noise in the data and the way that the Kriging response surface model has interpolated the data. A smoother response surface model can be generated using regression [36]
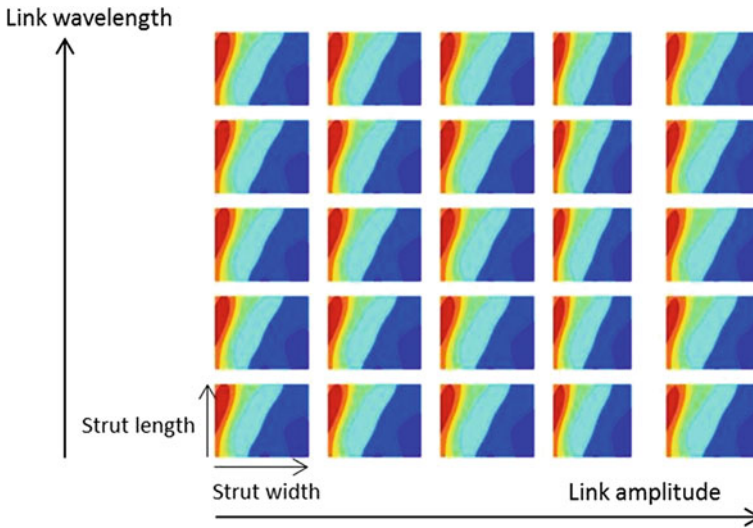
Fig. 12 Response surface model for non-dimensional recoil. Each inner tile has strut width on the abscissa and strut length on the ordinate. The separate tiles are plotted for fixed values [0.00, 0.25, 0.50, 0.75, 1.00] of the non-dimensional wavy link parameters: effective amplitude on the (outer) abscissa and effective wavelength on the (outer) ordinate. Further details can be found in [25]
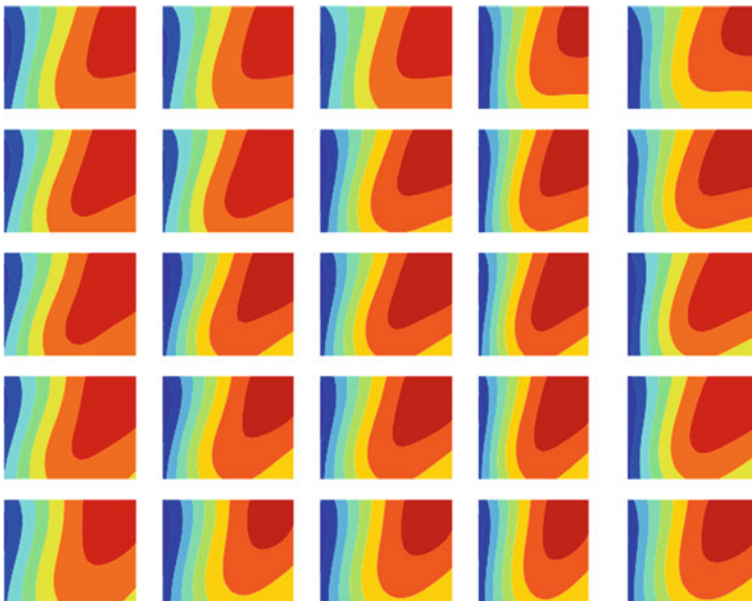

Fig. 13 Response surface model for non-dimensional tissue stress. See caption for Fig. 12
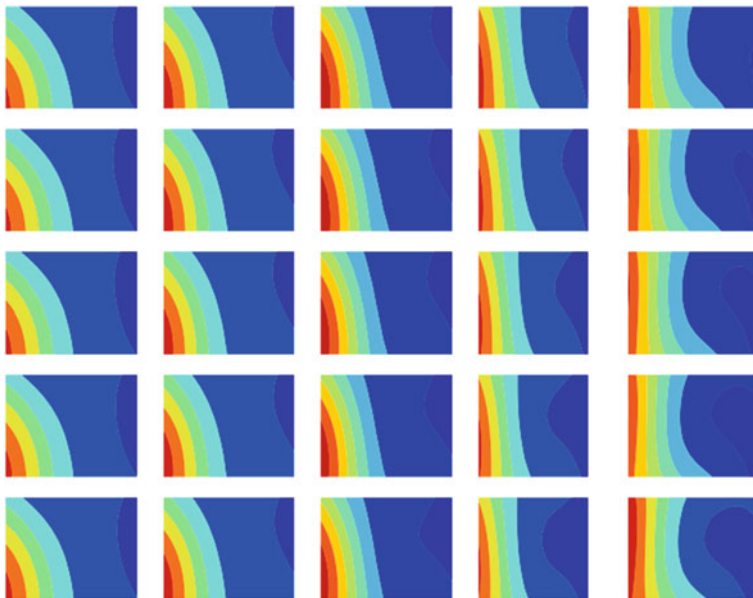
Fig. 14 Response surface model for non-dimensional tissue drug concentration. See caption for Fig. 12

and an example is available in [37] along with a discussion that helps to explain the noise in the data. In essence, when the links deform under load, they can come into self-contact, and this distorts the moment–curvature profile used to extract the flexibility metric. Despite this problem, flexibility is shown to be primarily dependent on the outer abscissa parameter that defines the link amplitude, as evidenced by the fact that individual tiles change far more significantly in Fig. 15 from left to right than they do from bottom to top. Furthermore, a flexibility improvement of 14 %, relative to the baseline design, was demonstrated in [25] without a decrease in the other objectives.

5 A Real Design Case

Based on the knowledge gained in earlier studies [21, 25], a DSO project was undertaken to design a biodegradable polymer stent which was to become the first prototype of the *Arterius Biodegradable Scaffold* (*ABS*), Arterius Ltd. This design cycle needed to be completed within 6 months. Starting from an initial concept, a parametric CAD model was constructed and developed during preliminary design. The process of setting up and developing the CAD model occupied most of the time of problem setup. In contrast, since a range of simulation models were available from other studies of metallic stents [21, 25], relatively modest effort was
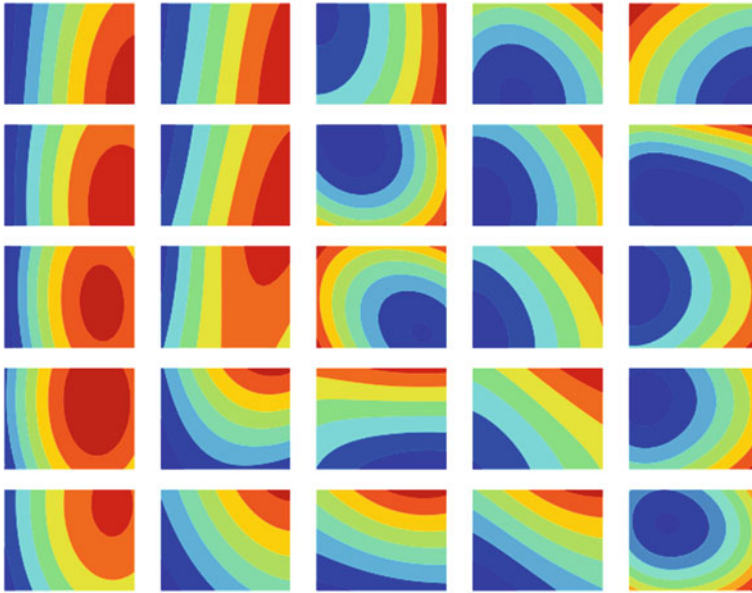
Fig. 15 Response surface model for non-dimensional flexibility. See caption for Fig. 12

needed to modify the associated simulation models for the study of the biodegradable scaffold. The design concept is the subject of an ongoing patent application, so specific details cannot be provided here. Nonetheless, it can be revealed that four design parameters were used including strut width and one related to the shape of the crowns. The strut thickness was fixed at 150 μm. Despite the lack of detail, this test case provides valuable insight to a real coronary artery design problem.

A 78 % symmetric constriction was used, comprising a Neo-Hookean representation of the single constituent plaque, inside a single layer of arterial tissue, similar to the setup described in Sect. 4.3. Although symmetry is exploited here for the demonstration purposes, in reality most coronary plaques are eccentric. Each CAD scaffold model was imported into an Abaqus assembly and placed inside the constriction (i.e. no stent positioning step was needed). Then, using Abaqus Explicit 6.9-1, separate steps were performed to simulate crimping onto a balloon-catheter followed by balloon expansion. In both steps, loading and relaxation were included using a smooth step profile. At the end of each simulation, metrics were extracted for the minimum lumen area (*MLA*) and the average recoil. A third measure of performance was obtained for the predicted drug distribution by running the steady state heat diffusion analogue in Abaqus Standard 6.9.1. Finally, a separate simulation was performed on the crimped stent (again in Abaqus Standard 6.9.1) to extract a fourth metric for the flexibility. Further details concerning the setup of these simulations are available in [25].
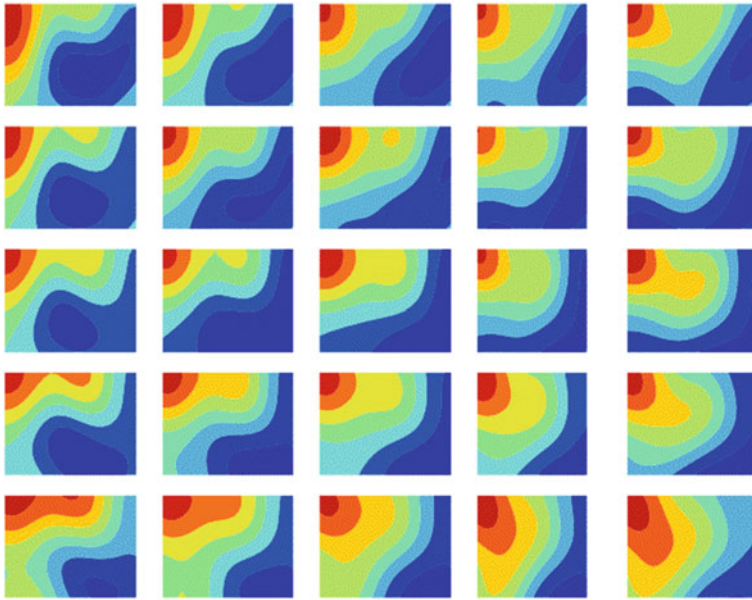
Fig. 16 Response surface model for non-dimensional inverse of minimum lumen area. The abscissa on each small tile represents non-dimensional strut width. The ordinate on each small tile denotes a non-dimensional parameter related to the shape of the crowns and each tile signifies fixed values [0.00, 0.25, 0.50, 0.75, 1.00] of the third and fourth parameters (which cannot be disclosed due to intellectual property protection)

So, the multi-objective problem comprised four input geometry parameters and four output objectives. In the time available for simulation, it was decided to run a 40 point design sample to gain an understanding of the multi-objective design space. Some of this data resulted in the response surface models shown in Figs. 16, 17.

The response surface model for the inverse of *MLA* is shown in Fig. 16. The inverse is used so as to treat each objective as a minimization problem. Each tile represents a slice through the non-dimensional *1/MLA* design space for fixed values [0.00, 0.25, 0.50, 0.75, 1.00] of the other two non-dimensional geometry parameters. Since all tiles are very similar, these two parameters have little effect on *MLA*. However, within each tile, favourable values of *MLA* are observed for high values of strut width (shown on the abscissa) and for low values of the ordinate. This follows a similar pattern to that shown in Fig. 12 and, again, wider struts predict greater radial support.

Also echoing the findings in [25], volume averaged tissue stress (*VAS*) exhibits a response that is in competition with *MLA* as depicted in Fig. 17. It is desirable to minimize tissue stress and, based on the definition of *VAS* [21], low stress occurs for low strut width, due to the lower stent-to-artery ratio of narrow struts and the associated reduced load needed to support the higher recoil in the vessel.

Combined in a multi-objective plot, the relationship between *MLA* and tissue stress can be more readily interpreted as in Fig. 18, wherein each point signifies an
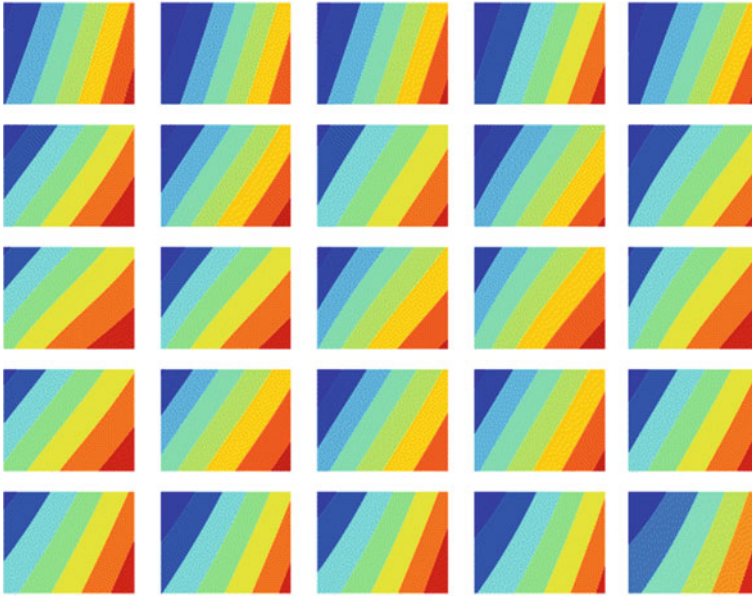
Fig. 17 Response surface model for non-dimensional volume averaged tissue stress (see caption for Fig. 16)

individual design. For example, designs 11 and 29 have wide struts that provide good radial support but at the expense of high tissue stress, whereas designs 8 and 32 generate lower tissue stress but have lower *MLA* (i.e. at higher *1/MLA*).

Of the designs that lie on the Pareto front, designs 24 and 17 bound an envelope of geometries that offer a balanced trade-off between *1/MLA* and tissue stress. When the full data-set was assessed (i.e. including the values of average recoil and flexibility) and combined with visual assessment of performance, it was decided to select design 17 as the prototype to be manufactured and tested. The width of design 17 was very close to 150 μm.

The prototype was manufactured by laser cutting the design from a PLLA tube. Preliminary bench tests demonstrated that the device could be successfully crimped and free-expanded on a balloon-catheter. However, tests of the radial strength of the expanded device revealed a problem in the design, wherein less than satisfactory support was provided at the ends of the device. Indeed, this helped to explain why levels of tissue stress were significantly lower than those obtained from the model of the *BVS-B* device. In effect, the optimizer had guided the process towards designs that imparted low tissue stress at the ends due to the way that these devices were able to adjust to the shape of the deformed vessel. This is a common feature in DSO methods wherein the optimizer can exploit weaknesses/deficiencies in the analysis setup.

A re-design of the *ABS* was needed and a further computational test was constructed to simulate collapse resistance when the expanded device was exposed to
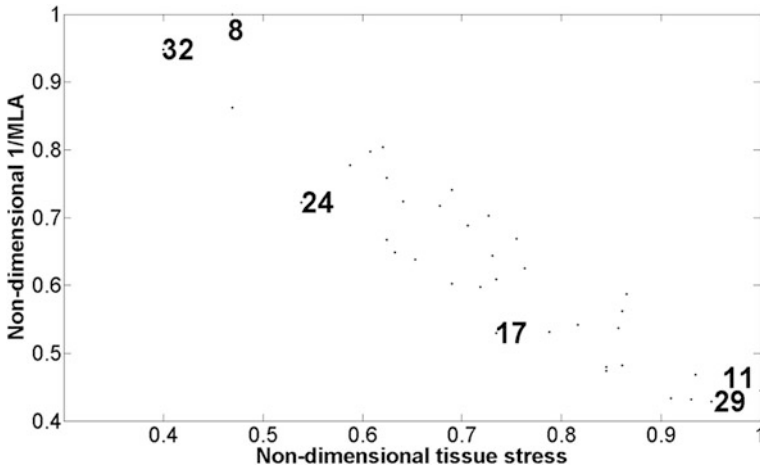
Fig. 18 Non-dimensionalized multi-objective plot of *1/MLA* versus tissue stress

an outer collapse load. This involved increasing (from zero) the pressure applied to the outer surfaces of the stent and monitoring the minimum stent diameter (*MSD*).

The poor overall radial strength of design 17 was confirmed with *MSD* beginning to decrease noticeably *at* 0.65 bar with complete collapse occurring just below 1 bar. In contrast, the *BVS-B* model was able to sustain its shape reasonably well up to approximately 0.95 bar with collapse at 1 bar.

At this stage, it was agreed to spend additional time (beyond the original 6 months) redesigning the *Arterius Biodegradable Scaffold*. Both the width and the thickness were fixed at 150 μm, and modified bounds were applied to the other three parameters. Another design cycle was conducted in which a further eight configurations were tested for *MLA*, tissue stress, flexibility and collapse resistance. The collapse test was added as a quasi-static step in the Abaqus Explicit simulation such that it was applied to the deformed shape produced during the expansion step. The optimal design, selected for manufacture and testing as the second prototype, had similar performance to design 17 in terms of *MLA*, tissue stress and flexibility but was significantly superior in terms of overall radial strength as predicted by the collapse test. A 20 % improvement in radial strength was produced with collapse occurring at approximately 1.2 bar. At the time of writing, the second prototype is about to be laser-cut from tubes manufactured by Arterius Ltd; the tubes used for the first prototype were sourced from elsewhere.

6 Summary and Conclusions

At a time when the design of coronary artery stents would appear to have reached a relatively mature evolutionary stage, geometrically at least, this chapter has sought to highlight how the knowledge gained to date can be exploited in the design of the

new generation of bioresorbable scaffolds. Currently, the main challenge is to reduce strut dimensions. Most bioresorbable devices have strut thicknesses and widths that are close to twice the corresponding dimensions of permanent metallic stents.

Whilst there is compelling clinical evidence from the ISAR-STEREO trials [14] and elsewhere [26] for reduced restenosis with thinner struts, less has been reported concerning the effect of strut width. Nakatani et al. have reported greater neo-intimal hyperplasia and poorer stent coverage associated with relatively wider struts [38]. However, these findings suffer from uncertainty concerning the main cause(s) of the effects since the narrow and wide struts are defined on one and the same *Cypher* stent platform by the wavy links and rings, respectively. Each strut type generates very different flow patterns and shear stresses on the vessel wall and this is known to influence tissue response.

An earlier study by Sullivan et al. [39] demonstrated that damage to the internal elastic lamina (IEL) is critically linked to higher incidence of myointimal hyperplasia and restenosis. Effectively, low profile struts that reduce local stress concentrations are needed so as to minimize abnormal stresses and mechanical damage to the tissue.

So, although wider struts offer greater radial support and larger contact area for drug delivery, most available evidence suggests that tissue damage caused by larger struts is the dominant effect leading to restenosis. However, it is to be noted that thinner struts may cause poor outcomes if they penetrate the tissue and rupture the IEL, possibly due to complications in the stenting procedure, combined with the fact that lower surface area contact may produce higher pressure loading.

Although many computational studies of stent geometry tend to fix strut thickness and assess the effect of strut width, Harewood et al. [30] used an FEA analysis of a simplified single half ring with five parameters, including both width and thickness, and showed that optimal values of width and thickness were reduced by 22 % and increased by 4 %, respectively, when optimizing radial stiffness.

Based on the observations above, future design studies should, if possible, consider the variation of both width and thickness, or other forms of strut cross-section parameterization, combined with other parameters defining the stent topology.

When designing the *Arterius Biodegradable Scaffold*, a time limited, computationally intensive study was conducted that led to the manufacture and testing of a first prototype within 6 months. Following laboratory tests, a shorter study of approximately 3 months culminated in modest re-design and a second prototype. The computational experiments involved four geometry parameters (including strut width and one for the shape of the crowns) and four objectives for design of the first prototype with a further objective—the direct test of radial strength—being added in the subsequent re-design phase. Throughout, strut thickness was kept constant at 150 μm and the multi-objective optimization procedure resulted in a potentially optimal design with an approximately square profile for the strut cross-section.

In contrast to the computationally expensive simulations employed in the Arterius study, Wu et al. applied two-dimensional FEA based optimization to models of the Biotronik biodegradable magnesium alloy stent (*MAS*), complemented by manufacture and testing, and identified four configurations for full three-dimensional simulations. Relative to a baseline design, improved performance (including reduced maximum principal strains and greater radial strength) was demonstrated in the three-dimensional models [35].

These two studies illustrate how computational design methods can be used to develop improved coronary stent designs. The *ABS* study used conceptual and preliminary design to prepare a platform that is nearly ready for pre-clinical trials. The work by Wu et al. was motivated by clinical evidence that had shown severe lumen loss after 4 months. Improved strut dimensions, including wider strut width, were identified that should extend degradation time and enhance radial scaffolding. In both studies, laboratory experiments were used to validate and complement the computational simulations and animal testing was completely avoided. Further mechanical testing will be required and, even though animal models will have to be employed in pre-clinical trials, the *MAS* re-design process illustrates that further re-design can be undertaken computationally (with complementary mechanical testing), again reducing the amount of animal testing that will be necessary.

With respect to biodegradable stents, the key challenge is to develop new materials or to enhance existing ones such that strut dimensions can be reduced. There is, approximately, two orders of magnitude stiffness mismatch between polymers and metal alloys. Sufficient polymer strengthening may ultimately be achieved by temperature controlled extrusion methods or by the use of additives or by using combinations of different materials.

More generally, stent evolution faces a number of other challenges. Even the most advanced metallic devices available today cannot avoid restenosis and thrombosis in all cases. Significant challenges still exist to overcome problems associated with malapposition, under-deployment, vessel tapering and bifurcation stenting. Lee et al. [40] have described the development of an early biodegradable bifurcation stent with comparable mechanical properties to metallic devices, but with very large struts. Ultimately, the only way to overcome these challenges may be through patient-specific stent design, a process likely to be made possible when supported by computational engineering methods and very powerful computers.

The main purpose of this chapter was to highlight a number of the design issues that are typically confronted when performing multi-objective design optimisation. By way of example, non-dimensional data was presented from a previous design study in a way to highlight how response surface models can be assessed for a range of objectives. Then, to illustrate how the same technology could be used in a time limited, industrially relevant design study, key elements of the design of a biodegradable device were presented. Unfortunately, details of the geometry could not be shown due to commercial sensitivity. However, the realities associated with the need to manufacture a prototype were outlined, starting from the findings from a preliminary study depicted in Figs. 16, 17, 18 and culminating in a more ad hoc re-design with consideration of radial collapse resistance. Finally, although the

value of multi-dimensional response surfaces has been demonstrated, more detailed assessment of the sensitivity of different objectives is sometimes necessary as well.

References

1. Onuma, Y., Serruys, P.W.: Bioresorbable scaffold: the advent of a new era in percutaneous coronary and peripheral revascularization? Circulation **123**, 779–797 (2011)
2. Stefanini, G.G., Holmes, D.R.: Drug eluting coronary artery stents. N. Engl. J. Med. **368**, 254–265 (2013)
3. Serruys, P.W., et al.: A comparison of balloon-expandable-stent implantation with balloon angioplasty in patients with coronary artery disease. N. Engl. J. Med. **331**, 489–495 (1994)
4. Serruys, P.W., et al.: Angiographic follow-up after placement of a self-expanding coronary-artery stent. N. Engl. J. Med. **324**, 13–17 (1991)
5. van der Giessen, W.J., Slager, C.J., van Beusekom, H.M., van Ingen Schenau, D.S., Huijts, R.A., Schuurbiers, J.C., de Klein, W.J., Serruys, P.W., Verdouw, P.D. Development of a polymer endovascular prosthesis and its implantation in porcine arteries. J. Interv. Cardiol. **5**, 175–185 (1992)
6. van der Giessen, W.J., Lincoff, A.M., Schwartz, R.S., van Beusekom, H.M., Serruys, P.W., Holmes Jr, D.R., Ellis, S.G., Topol, E.J.: Marked inflammatory sequelae to implantation of biodegradable and non-biodegradable polymers in porcine coronary arteries. Circulation **94**, 1690–1697 (1996)
7. Tamai, H., Igaki, K., Kyo, E., et al.: Initial and 6-month results of biodegradable poly-l-lactic acid coronary stents in humans. Circulation **102**, 399–404 (2000)
8. Ormiston, J.A., Serruys, P.W.S.: Bioabsorbable coronary stents. Circ. Cardiovasc Intervent. **2**, 255–260 (2009)
9. Nishio, S. et al.: Long-term (>10 years) clinical outcomes of first-in-man biodegradable poly-*l*-lactic acid coronary stents: Igaki-Tamai stents. Circulation **125**(19), 2343–2353 (2012)
10. Strandberg, E., Zeltinger, J., Schultz, D.G., Kaluza, G.L.: Late positive remodeling and late lumen gain contribute to vascular restoration by a non-drug eluting bioresorbable scaffold: a four-year intravascular ultrasound study in normal porcine coronary arteries. Circ. Cardiovasc. Interv. **5**(1), 39–46 (2012)
11. Gomez-Lara, J., Diletti, R., Brugaletta, S. et al.: Angiographic maximal luminal diameter and appropriate deployment of the everolimus-eluting bioresorbable vascular scaffold as assessed by optical coherence tomography: an ABSORB cohort B trial sub-study. Eurointervention **8**(2), 214–224 (2012)
12. Hanratty, C.G., Walsh, S.J.: Longitudinal compression: a "new" complication with modern coronary stent platforms—time to think beyond deliverability. Eurointervention **7**(7), 872–877 (2011)
13. Prabhu, S., Schikorr, T., Mahmoud, T., Jacobs, J., Potgieter, A., Simonton, C.: Engineering assessment of the longitudinal compression behaviour of contemporary coronary stents. Eurointervention **8**(2), 275–281 (2012)
14. Kastrati, A., Mehilli, J., Dirschinger, J., et al.: Intracoronary stenting and angiographic results: strut thickness effect on restenosis outcome (ISAR-STEREO) trial. Circulation **103**, 2816–2821 (2001)

15. Kreutzer, J., Rome, J.J.: Open-cell design stents in congenital heart disease: a comparison of Intrastent vs Palmaz stents. Cath. Cardio. Int. **56**, 400–409 (2002)
16. Stoeckel, D., Bonsignore, C., Duda, S.: A survey of stent designs. Min. Invas. Ther & Allied Technol. **11**(4), 137–147 (2002)
17. Serruys, P.W., Rensing, B.J.: Handbook of coronary stents. Dunitz (2002)
18. Amoroso, G., van Geuns, R-J., Spaulding, C. et al.: Assessment of the safety and performance of the STENTYS self-expanding coronary stent in acute myocardial infarction: results from the APPOSITION I study. Eurointervention **7**, 428–436 (2011)
19. Bourantas, C.V., Zhang, Y., Farooq, V., Garcia–Garcia, H.M., Onuma, Y., Serruys, P.W.: Bioresorbable scaffolds: current evidence and ongoing clinical trials. Curr. Cardiol. Rep. **14**, 626–634 (2012)
20. Durand, E., Lemitre, M., Couty, L., Sharkawi, T., Brasselet, C., Vert, M., Lafont, A.: Adjusting a polymer formulation for an optimal bioresorbable stent: a 6-month follow-up study. Eurointervention **8**(2), 242–249 (2012)
21. Pant, S., Limbert, G., Curzen, N., Bressloff, N.W.: Multi-objective design optimisation of coronary stents. Biomaterials **32**, 7755–7773 (2011)
22. Mortier, P., Holzapfel, G. A., De Beule, M. et al.: A novel simulation strategy for stent insertion and deployment in curved coronary bifurcations: comparison of three drug-eluting stents. Ann. Biomed. Eng. **38**(1), 88–99 (2010)
23. Migliavacca, F., Gervaso, F., Prosi, M., Zunino, P., Minisini, S., Formaggia, L., Dubini, G.: Expansion and drug elution model of coronary stent. Comp. Meth. Biomech. Biomed. Eng. **10**, 63–73 (2007)
24. Grogan, J.A., Leen, S.B., McHugh, P.E.: Comparing coronary stent material performance on a common geometric platform through simulated bench testing. J. Mech. Behav. Biomed. Mat. **12**, 129–138 (2012)
25. Pant, S., Bressloff, N.W., Limbert, G.: Geometry parameterization and multidisciplinary constrained optimisation of coronary stents. Biomech Mod. Mechanobiology **11**(1), 61–82 (2011)
26. Holzapfel, G.A., Stadler, M., Gasser, T.C.: Changes in the mechanical environment of stenotic arteries during interaction with stents: computational assessment of parametric stent designs. J. Biomech. Eng. **127**, 166–180 (2005)
27. Gijsen, F.J.H., Migliavacca, F., Schievano, S., et al.: Simulation of stent deployment in a realistic human coronary artery. BioMed. Eng. Online **7**, 23 (2008)
28. Hicks, R., Henne, P.: Wing design by numerical optimization. J. Aircraft **15**(7), 407–412 (1978)
29. Pant, S., Bressloff, N.W., Forrester, A.I.J., Curzen, N.: The influence of strut-connectors in stented vessels: a comparison of pulsatile flow through five different coronary stents. Ann. Biomed. Eng. **38**(5), 1893–1907 (2010)
30. Harewood, F., Thornton, R., Sharp, P.: Step change in design: exploring sixty stent design variations overnight. www.altairproductdesign.com 2011
31. Sobester, A., Leary, S.J., Keane, A.J.: On the design optimization strategies based on global response surface approximation models. J. Glob. Opt. **33**, 31–59 (2005)
32. Jones, D.R.: A taxonomy of global optimization methods based on response surfaces. J. Glob. Opt. **21**(4), 345–383 (2001)
33. Krige, D.G.: A statistical approach to some basic mine valuation problems on the Witwatersrand. J. Chem. Mett. Min. Soc. SA. **52**(6), 119–139 (1951)
34. Forrester, A. I. J., Sóbester, A., Keane, A. J.: Engineering design via surrogate modelling: a practical guide. Wiley, Chichester (2008)
35. Wu, W., Petrini, L., Gastaldi, D., Villa, T., Vedani, M., Lesma, E., Previtali, B, Migliavacca, F.: Finite element shape optimization for biodegradable magnesium alloy stents. Ann. Biomed. Eng. **38**(9), 2829–40(2010)
36. Forrester, A.I.J., Keane, A.J., Bressloff, N.W.: Design and analysis of noisy computer experiments. AIAA J. **44**(10), 2331–2339 (2006)

37. Pant, S.: Multidisciplinary and multiobjective design of coronary stents. PhD Thesis, University of Southampton, UK (2012)
38. Nakatani, S., Nishino, M., Taniike, M. et al.: Initial findings of impact of strut width on stent coverage and apposition of sirolimus-eluting stents assessed by optical coherence tomography. Cath. Cardo. Int. (2012)
39. Sullivan, T.M., Ainsworth, S.D., Langan, E.M., et al.: Effect of endovascular stent strut geometry on vascular injury, myointimal hyperplasia and restenosis. J. Vasc. Surg. **36**(1), 143–149 (2002)
40. Lee, C.-H., Chen, C.-J., Liu, S.-J., Hsiao, C.-Y., Chen, J.-K.: The development of novel biodegradable bifurcation stents for the sustainable release of anit-proliferative sirolimus. Ann. Biomed. Eng. **40**(9), 1961–1970 (2012)